Journal of Power Sources 195 (2010) 1657–1666

Contents lists available at ScienceDirect

Journal of Power Sources

journal homepage: www.elsevier.com/locate/jpowsour

The impact of steam and current density on carbon formation from biomass gasification tar on Ni/YSZ, and Ni/CGO solid oxide fuel cell anodes

Joshua Mermelstein[a], Marcos Millan[a], Nigel Brandon[b,*]

[a] Chemical Engineering, Imperial College London, SW7 2AZ, United Kingdom
[b] Earth Science Engineering, Imperial College London, Prince Consort Road, RSM Building, London SW7 2AZ, United Kingdom

ARTICLE INFO

Article history:
Received 17 August 2009
Received in revised form
15 September 2009
Accepted 17 September 2009
Available online 26 September 2009

Keywords:
Solid oxide fuel cell (SOFC)
Biomass gasification
Tars
Carbon deposition
Steam
Current density

ABSTRACT

The combination of solid oxide fuel cells (SOFCs) and biomass gasification has the potential to become an attractive technology for the production of clean renewable energy. However the impact of tars, formed during biomass gasification, on the performance and durability of SOFC anodes has not been well established experimentally. This paper reports an experimental study on the mitigation of carbon formation arising from the exposure of the commonly used Ni/YSZ (yttria stabilized zirconia) and Ni/CGO (gadolinium-doped ceria) SOFC anodes to biomass gasification tars. Carbon formation and cell degradation was reduced through means of steam reforming of the tar over the nickel anode, and partial oxidation of benzene model tar via the transport of oxygen ions to the anode while operating the fuel cell under load. Thermodynamic calculations suggest that a threshold current density of 365 mA cm^{-2} was required to suppress carbon formation in dry conditions, which was consistent with the results of experiments conducted in this study. The importance of both anode microstructure and composition towards carbon deposition was seen in the comparison of Ni/YSZ and Ni/CGO anodes exposed to the biomass gasification tar. Under steam concentrations greater than the thermodynamic threshold for carbon deposition, Ni/YSZ anodes still exhibited cell degradation, as shown by increased polarization resistances, and carbon formation was seen using SEM imaging. Ni/CGO anodes were found to be more resilient to carbon formation than Ni/YSZ anodes, and displayed increased performance after each subsequent exposure to tar, likely due to continued reforming of condensed tar on the anode.

1. Introduction

Significant quantities of biomass materials, such as agricultural and residual wastes, are generated throughout the world annually. Biomass fuels have substantial potential as a carbon neutral renewable energy source that can be used for the production of electricity and heat in combination with solid oxide fuel cells (SOFCs) [1–4], playing an important role in the mitigation of environmental impacts associated with increasing carbon emission from fossil fuels. The high operating temperatures and fuel flexibility of SOFCs allow the utilization and internal reforming of wide range of hydrocarbon based fuels. However, the impact of tars from the gasification process is not well understood experimentally. Previous results [5] showed that degradation of a SOFC anode occurred due to carbon formation when exposed to benzene as a model tar compound. This work seeks to study the mitigation of such carbon formation from benzene model gasification tar, in a syngas mixture containing H_2 and N_2, through steam reforming and partial oxidation under cell load using two types of commercially available SOFC anodes, nickel/yttria stabilized zirconia (Ni/YSZ) and nickel/gadolinium-doped ceria (Ni/CGO). Thermodynamically calculated threshold current densities are compared with experimental results.

1.1. Methods to reduce carbon formation

The presence of tar in the gas stream may condense leaving deposits on the walls of piping; enable polymerization of heavier poly-aromatic compounds [6]; affect the steam reforming of the syngas in to hydrogen [6,7]; and as a consequence lead to the shutdown of gasification process units due to blocking and fouling of downstream processes [8]. In thermodynamically unfavorable conditions the presence of tars will lead to carbon formation and severe degradation of nickel based SOFC anodes [5,9]. To prevent this from occurring, the literature suggests several methods to reduce carbon deposition and maintain anode performance, including optimizing anode microstructure and fuel cell operational characteristics such as the addition of steam and increased current density.

* Corresponding author. Tel.: +44 (0) 20 75945704; fax: +44 (0) 20 75947444.
E-mail address: n.brandon@imperial.ac.uk (N. Brandon).

0378-7753/$ – see front matter © 2009 Elsevier B.V. All rights reserved.
doi:10.1016/j.jpowsour.2009.09.046

1.1.1. Anode modification

Carbon deposition effects can be reduced by incorporating other materials into the SOFC anode. For example it has been found that ceria may enhance anode performance by promoting charge transfer reactions at the triple phase boundary, due to its mixed ionic electronic conductivity. He and Hill [10] reported that adding Zr-doped ceria to Ni/YSZ pellets was an effective way to reduce carbon formation. They found that the Zr-doped ceria prevented carbon filament growth after exposure to methane, and through Temperature Programmed Oxidation (TPO) experiments, found that significantly less carbon deposited on the sample.

Similarly, additions such as Ag, Cu, and molybdenum to nickel anodes (infiltrated by addition of species as nitrates or oxides prior to milling) have been found to substantially reduce the level of carbon deposition [11,12]. Additionally, it has been found that the synthesis path to manufacture the anode materials, the composition, as well as the microstructure of the anode, affects carbon deposition on anode materials [12]. For example, Gorte and Vohs [13] suggest that the mechanism for carbon formation on Cu differs from carbon formation on metals such as Ni, Co and Fe. With Ni catalysts the hydrocarbon cracks on the Ni surface, carbon is dissolved into the bulk metal and is precipitated at the nickel surface. Cu on the other hand was found to have a simpler mechanism, wherein carbon was only deposited on the surface of the catalyst, without the physical damage associated with Ni catalysts.

1.1.2. Addition of steam

Addition of steam has also been shown to reduce carbon formation on SOFC Ni anodes and Ni based anode materials via steam reforming [11,14]. However adding steam into a hydrocarbon fuel stream can decrease the power density at high steam concentrations, around steam to carbon ratios (S/C) of 2–3 [11,15,16], primarily due to a decrease in the OCV of the fuel cell at high steam contents.

1.1.3. Current density

Oxygen combines with electrons at the cathode forming oxide ions. The oxide ions transport through the electrolyte of the SOFC to the anode. As the current drawn from the SOFC increases, the flux of oxygen ions across the electrolyte correspondingly increases [11,17]. The increased conversion of carbonaceous species such as methane, and stepwise increase in CO, CO_2 and H_2O production with increasing current drawn, indicates that the partial oxidation of methane (or other carbonaceous species) by oxygen ions occurs [11,18] through the following reactions at the anode:

$$C_xH_y + \left(\frac{y}{2} + 2x\right) O^{2-} \leftrightarrow \frac{y}{2}H_2O + xCO_2 + (y + 4x)e^- \quad (1)$$

for any carbonaceous species, and:

$$C_nH_m + nH_2O \leftrightarrow nCO + \left(n + \frac{m}{2}\right) H_2 \quad (2)$$

for steam reforming.

Therefore the current density has a significant impact on carbon deposition from both light and heavy hydrocarbon fuels, as shown in this study, as it determines the amount of oxygen ions that are available at the anode for reaction [9].

1.1.4. Anode preparation and reduction

The performance of a nickel cermet anode is influenced by its morphology, triple phase boundary distribution, and Ni grain connectivity [19]. It has been shown that the microstructure of an anode sintered at lower temperatures resisted the effects of anode degradation from carbon as the high surface area of the nickel cermet did not readily allow for blockage of active sites from carbon deposition. This allowed for improved stability when operating on methane [20], though at the cost of anode performance. It was found that carbon deposition improved conductivity by linking Ni particles together with carbon [16,21]. However this observation may not be relevant to well percolated commercially available SOFC anodes as the conducting nature of carbon would not greatly contribute to improved conductivity over that of the metallic nickel. Reduction at higher temperatures (such as used in this study) allows for greater sintering, providing larger nickel particles, reduced surface area, and a more continuous nickel structure [20,22,23]. However the formation of a surface carbon layer could occur, hindering the transport of reactants to active sites and eventually leading to deactivation of the anode [20,24].

Clearly, the operating conditions (steam content, current density), composition, structure, and pretreatment of the anode will have a significant impact on its ability to resist carbon formation. As within other aspects of catalysis, a catalyst designed for steam reforming may not be appropriate for partial oxidation, and in addition this can also vary depending on the fuel used. It would therefore be appropriate to use a similar approach for selecting an anode that is resistant to carbon formation when using a biomass gasification syngas containing tar. The impact of anode exposure to benzene as a model tar compound arising from biomass gasification over two commercially available SOFC anodes is examined in this work, operating at open circuit and under load, and as a function of steam content.

2. Experimental

2.1. Experimental set-up

A SOFC test station has been developed to test the carbon deposition characteristics of synthetically generated biomass gasification tars over nickel anode materials, and to study the effects of tars on operating SOFCs, as shown in Fig. 1. This test station has the capability of generating synthetic biomass gasification syngas using pure N_2, H_2, CO, CO_2, and methane by mixing to the desired partial pressures using a Fideris FCTS GMET mass flow control unit. To isolate the carbon formation from tars, CO, CO_2, and methane were not used in this study as these components may contribute to additional carbon formation and/or additional oxidation behavior via CO_2 reforming and steam production from the reverse water gas shift (RWGS) reaction. Therefore, to identify the effect of steam on carbon formation from biomass gasification tar, only the fraction of hydrogen represented in Table 1, describing the typical properties of a syngas from biomass gasification [7,25–29], was used with a flow rate of 15 ml min^{-1} H_2 mixed with 85 ml min^{-1} N_2 (purity >99.999%, BOC gases). The synthetic mixture is passed through a temperature controlled water bath for gas humidification, or directly to a heated line to study the effect of dry gas on the system. The gas enters a heated and insulated line which contains an injection port to introduce synthetic model tars via a syringe pump (KD Scientific) at a rate of 102 μl h^{-1}, producing a tar concentration of 15 g N m^{-3}. A portion of the tar injection line is heated at temperatures slightly above the boiling point of the model tar com-

Table 1
Typical properties of biomass gasification syngas.

Compound	Gas (vol.%) [26]	Dry gas (ave. vol.%)[a]
H_2	14.5	15
CO	21.0	24
CO_2	9.7	11
H_2O	4.8	–
CH_4	1.6	2
N_2	48.4	48

[a] Average from literature data.

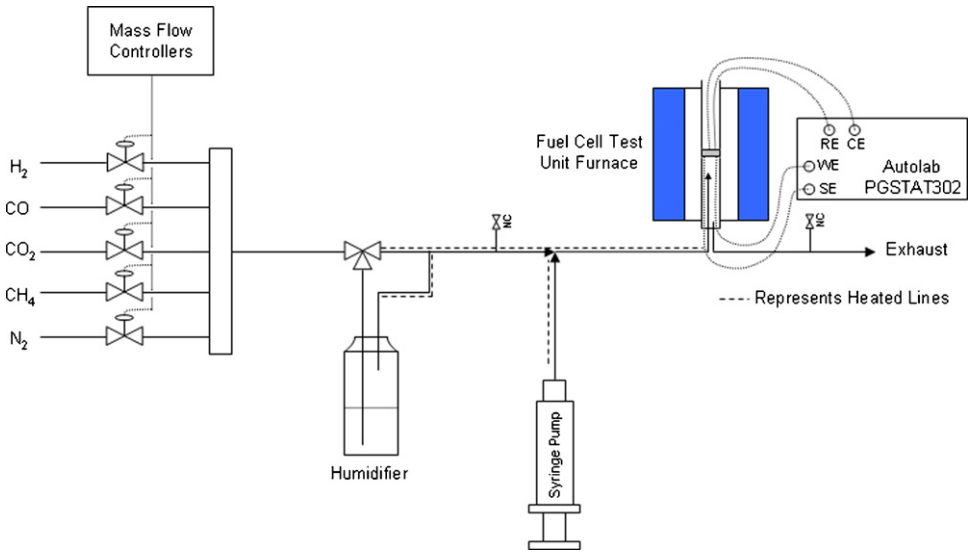

Fig. 1. Schematic illustration of the SOFC test station.

pound to allow for vaporization of the tar species into the gas phase, and subsequent mixing with the incoming syngas. Downstream, the tar-containing syngas is fed to a heated furnace containing the SOFC. The discharge from the reactor is sent to a mass spectrometer and gas chromatograph for gas stream analysis.

2.2. SOFC button cell preparation

An electrolyte supported button cell was prepared in order to assess anode performance under varying load and steam conditions in the presence of biomass gasification model tars. Yttria-stabilized zirconia (YSZ) pellets were prepared by pressing 3 g of YSZ (TZ-8Y Zirconia, Tosoh Corporation) powder at 1 tonne pressure for 30 s, before firing at 1450 °C for 5 h at a ramp rate of 5 °C min^{-1}. The pellets were polished using 1200 grit polishing paper to ensure uniform thickness of ~1.4 mm prior to screen printing the anode and cathode on the electrolyte. Nickel oxide cermet ink (60:40 NiO/YSZ or 50:50 NiO/CGO by weight, FuelCellMaterials, USA) as the anode, and LSM–YSZ (50:50 $(La_{0.80}Sr_{0.20})_{0.98}MnO_{3-x}/(Y_2O_3)_{0.08}(ZrO_2)_{0.92}$ by weight, FuelCellMaterials, USA) as the cathode and reference electrode, were screen printed (error of ±125 μm in the placement of electrode geometries) and fired sequentially at 1300 and 1150 °C, respectively. The anode was a circular disk 1.1 cm in diameter with a cross-sectional area of 0.95 cm^2 and the cathode was an identical circular disk, surrounded by a reference electrode with an internal diameter of 17 mm, and an external diameter of 19 mm.

2.3. SOFC performance testing

The fuel cells were tested in a button fuel cell test unit capable of testing fuel cells with diameters of 22–30 mm that was placed within the heated furnace of the test station described above. A description of this test station can be found in Offer et al. and Mermelstein et al. [5,30]. The cell was taken up to an operating temperature of 765 °C at a ramp rate of 7.5 °C min^{-1} with the anode side exposed to an inert atmosphere. Anode reduction took place by exposing the catalyst at operating temperature in 2.5% humidified steam and 5% H_2 for 30 min, then increasing incrementally to 25% H_2 balance N_2 over a period of 30 min at a flow rate of 50 ml min^{-1}. The sample was then held in 25% H_2 for 30 min. After reduction, flow was increased to 100 ml min^{-1} and the hydrogen concentration changed to the experimental operating conditions of 15% H_2 and the experiment's appropriate steam content. For the electrochemical measurements, an Autolab PGSTAT302 (Eco Chemie BV, The Netherlands) with an FRA module was used. The electrochemical impedance response was measured in the frequency range 0.1 Hz to 10 kHz with five points measured at each decade, and a stimulus potential amplitude of 0.02 V (rms) was used throughout. Voltage current performance was measured using linear sweep voltammetry from the cell open circuit voltage (OCV) to an anode potential of −0.5 V, with a step potential of 0.00015 V and a scan rate of 0.01 V s^{-1}. Autolab FRA and GPES software was used to log and analyze the measurements.

Measured anode overpotential is dependent on the series resistance of the anode plus electrolyte, described by the following equation and further explained in Offer et al. [30].

$$\eta_{anode} = \eta_{measured} - jR_s^{OCV} \quad (3)$$

where 'η' is the overpotential, 'j' is the current density in mA cm^{-2}, and 'R_s' is the series resistance measured at OCV. However errors are introduced when using this correction method for overpotential when dynamic changes in R_s and polarization resistance (R_p) occur, as is the case when carbon deposition occurs. Therefore, in this study, performance curves are expressed for anode potential, measured as the uncorrected potential difference between the anode and reference electrode, as a function of current density.

3. Results and discussion

3.1. Thermodynamic predictions—effect of current density on carbon formation

Thermodynamic calculations were carried out using HSC chemistry software (version 5.11, Outokumpu Research Oy, Finland) via the Gibbs free energy minimization method as described in Sasaki and Teraoka [31]. Calculations were conducted reflecting experimental operating conditions of 765 °C and 1 atm for a 1 cm^2 anode operating on 15 g m^{-3} benzene model tar in a 15% H_2 balance N_2 gas stream of 100 ml min^{-1}. The number of moles of oxygen (NO_2) transferred from the cathode to the anode used in the thermodynamic calculations was calculated by Faraday's law:

$$N_{O_2}(\text{mol cm}^{-2}\,\text{s}^{-1}) = \frac{j}{4F} \quad (4)$$

where j is the current density and F is the Faraday constant. To account for the flow rate of fuels supplied to the anode, the equi-

librium compositions are related to the fuel utilization, U:

$$U = \frac{i}{F\left(\sum_{i=1}^{n} n_{e_i} \times y_i\right) N_{Fuel}} \quad (5)$$

where i is the current in amps, n_e is the number of electrons from the oxidation reaction of component 'i', y is the fuel fraction of component 'i', and N_{Fuel} is the fuel flow rate in mol s^{-1} to the anode.

Fig. 2 shows the calculated downstream major gas phase components of H_2, CO, CO_2, H_2O, CH_4 (N_2 not shown) and carbon existing as a pure condensed phase, as a function of current density and fuel utilization. Fuel utilization is calculated up to 100% ($j = 3$ A cm^{-2}), while noting that in practice fuel utilization is generally limited to around 85% to prevent anode oxidation and mass transport limitations. The thermodynamic calculations reveal that the amount of $C_{(s)}$ which is caused by the decomposition of the gasification tar, is predicted to be maximum at open circuit. $C_{(s)}$ is reduced with increased load up to a current density of 365 mA cm^{-2} (equivalent to a fuel utilization of 12% for the conditions examined here) beyond which carbon deposition is no longer thermodynamically favored. This transition is known as the threshold current density and up to this point the primary mechanism for carbon removal and conversion of the carbonaceous species is by partial oxidation to syngas components of H_2 and CO [9,32]. Up to this transition point CH_4 exists at low concentration (<1.5×10^{-7} mol s^{-1}, 0.19%), there is little increase in H_2O, and H_2 exists at a constant concentration. CO increases significantly to a maximum value at the threshold current density. Equilibrium compositions of the gas mixture change abruptly after this point. Further increases in current density (and higher rate of oxygen supply) above this threshold requires more consumption of H_2 and CO for electrochemical oxidation to produce electricity, causing a rapid increase in CO_2 and H_2O concentration indicating the transition towards direct oxidation of carbonaceous species in the gas stream [33]. CH_4 is rapidly consumed, production of CO from partial oxidation is decreased, and hydrogen consumption, along with accompanying H_2O production, increases rapidly. Thermodynamic calculations assume a homogeneous gas mixture. However it should be noted that in a SOFC stack, P_{O_2} concentration gradients exist within the anode. This could result in localized carbon deposition arising from P_{O_2} gradients which are not taken into account in the calculations reported here.

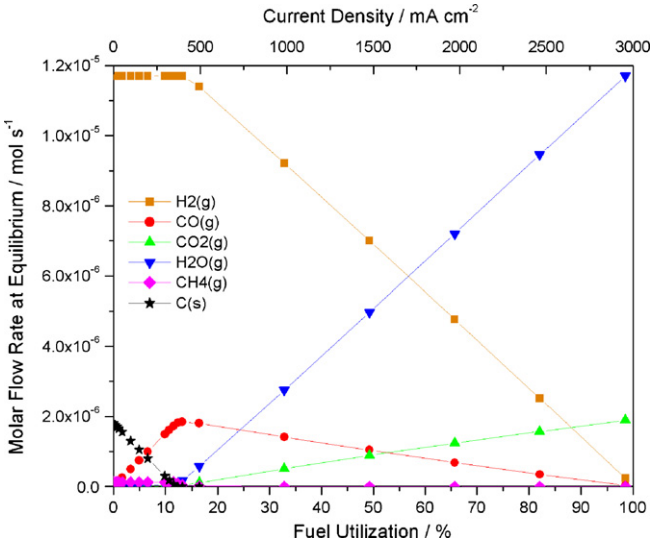

Fig. 2. Calculated equilibrium diagram of carbon and main species in the gas phase as a function of current density and fuel utilization for a 1 cm^2 anode operating on an inlet stream of 15 g m^{-3} benzene as model tar in dry 15% H_2 balance N_2 for a feed rate of 100 ml min^{-1} at a temperature of 765 °C.

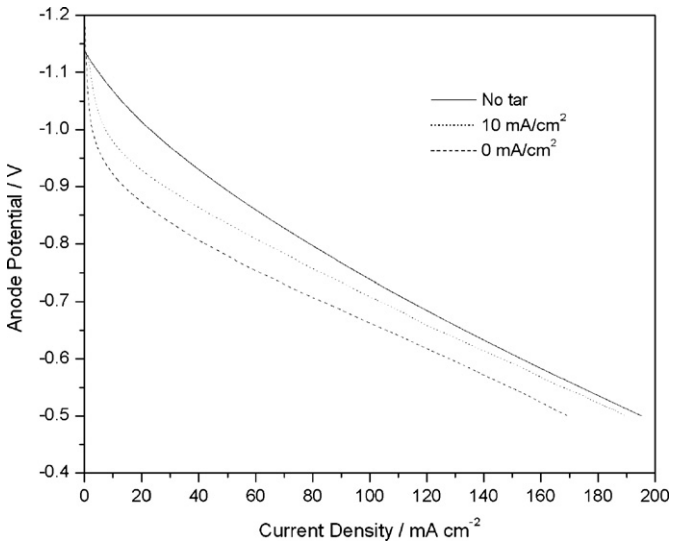

Fig. 3. Anode Potential of SOFC with Ni–YSZ anodes after exposure to 15 g m^{-3} benzene tar in a dry 15% H_2/N_2 atmosphere at 765 °C after operating at 0 and 10 mA cm^{-2} for 30 min compared with the initial performance of the cell before tar loading.

3.2. Current density effects on the performance of SOFCs exposed to benzene model tar in dry conditions

The increase in load drawn across a SOFC increases the concentration of O^{2-} ions at the anode which in turn allows the partial oxidation of carbonaceous species. As shown in Section 3.1, a threshold current density exists above which carbon formation is no longer predicted. Increasing current density above this point leads to direct oxidation of the carbonaceous fuel. The impact of these reactions can be seen in the effect of current density on the polarization curves and impedance characteristics of the Ni/YSZ based fuel cell as shown in Figs. 3 and 4, respectively.

The polarization curves measured at OCV of separate Ni/YSZ anodes after exposure to 15 g m^{-3} tar for 30 min at open circuit and at 10 mA cm^{-2} are compared with initial cell performance in Fig. 3. Here the polarization curves show the negative impact on anode kinetics from exposure to tar, though this negative impact is reduced by operating the cell under a load of 10 mA cm^{-2} compared to running the cell at OCV. Transport limitations in the polarization curve do not seem to be a factor in either case, and it is apparent the performance of the cell tends towards its initial value at higher current densities. This could be the result of carbon oxidation during acquisition of the polarization curve where:

$$C + 2O^{2-} \leftrightarrow CO_2 + 4e^- \quad (6)$$

and

$$C + O^{2-} \leftrightarrow CO + 2e^- \quad (7)$$

The amount of carbon consumed at the anode is directly proportional to the amount of electric charge, Q, passing through the circuit during polarization, calculated using Faraday's law where:

$$Q = \int_0^t j(t)dt \quad (8)$$

and

$$N_{C,cons} = \frac{Q}{nF} \quad (9)$$

for carbon oxidation occurring in both reactions (6) and (7). The total charge during polarization was 4.13 A s cm^{-2} which allows for the oxidation of 0.385 mg of carbon in dry conditions. In comparison, as found in previous results [14], this is approximately

equivalent to the amount of carbon that would occur in the presence of 5% steam. The high amount of carbon found on the anode in dry conditions, acts as a fuel, allowing for slight improvements in performance at the higher current densities, shown in Fig. 3. This may indicate that during anode polarization, high current densities may be oxidizing carbon off the anode.

The effect of current density on the impedance characteristics for Ni/YSZ fuel cells are shown in Fig. 4, where 15 g m^{-3} benzene tar was fed to the fuel cell in dry 15% H_2 operating at current densities of 5–350 mA cm^{-2} for 30 min. At the end of 30 min the cell was placed back at open circuit in the absence of tars to obtain an impedance spectrum. The initial impedance spectra, not shown, had a series resistance of 2–3 Ω cm^2 with an average polarization resistance of 7 Ω cm^2. Cell degradation rates were observed at 0.27 and 0.59 Ω cm^2 h^{-1} for R_s and R_p, respectively. Fig. 4a shows that, as the operating current density is increased, the cell impedance (taken at open circuit after 30 min tar exposure at that current density) is reduced, hence it is clear that the increased current density is reducing anode degradation arising from the formation of carbon. Furthermore, this trend in reduced anode degradation can be seen in Fig. 4b, showing the polarization resistances as measured at OCV after exposure to tars under increasing current density. As the current density is increased towards that of the threshold current density, the degradation of the cell, measured as the increase

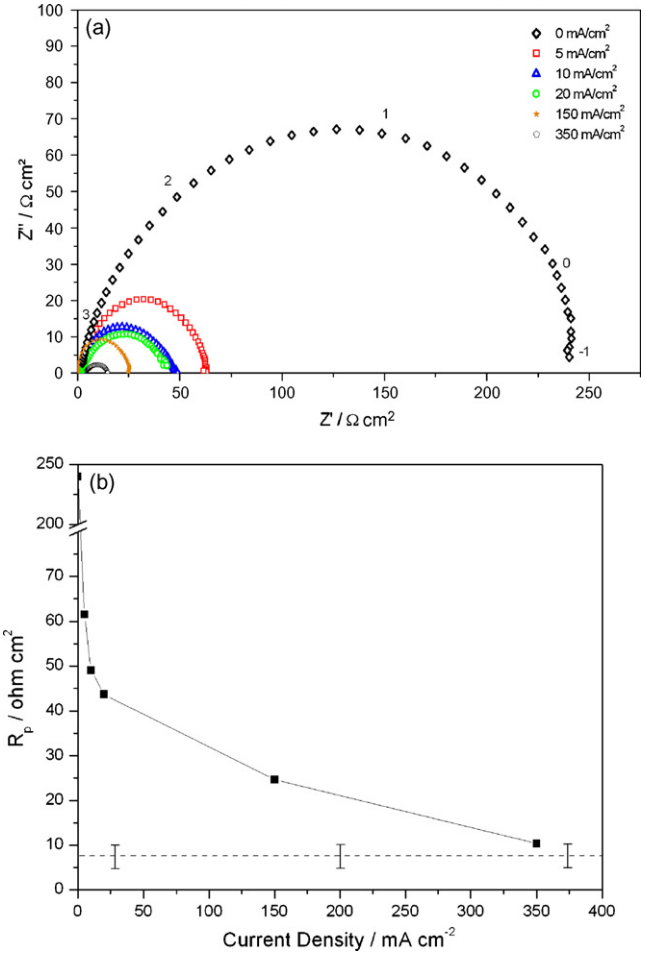

Fig. 4. (a) Effect of cell load from OCV to 350 mA cm^{-2} on the impedance spectra of SOFCs with similar Ni–YSZ anodes operating at 765 °C in a 15% H_2 atmosphere exposed to 15 g m^{-3} benzene for 30 min. Log scale frequencies are presented next to the 0 mA cm^{-2} plot. All spectra were measured at open circuit after interrupting the flow of current. (b) Ni/YSZ anode polarization resistances after exposure to 15 g m^{-3} benzene model tar for 30 min at 765 °C under load between 0 and 350 mA cm^{-2} in a dry 15% H_2 atmosphere, measured at OCV. (- - -) Average initial R_p.

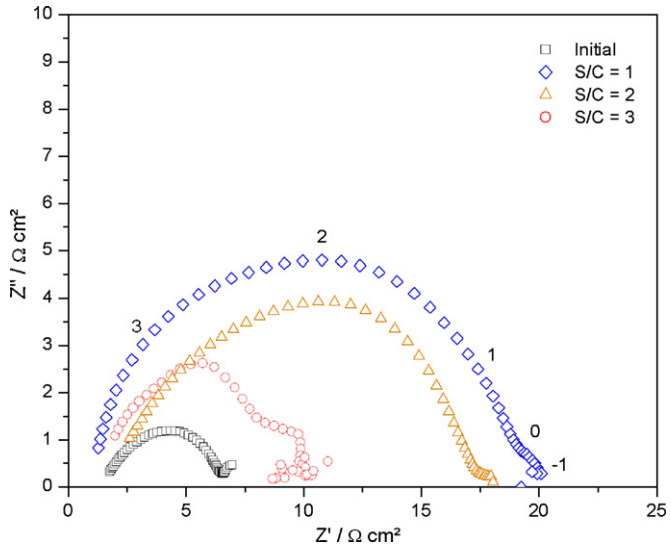

Fig. 5. Impedance spectra of SOFCs at OCV with similar Ni–YSZ anodes operating at 765 °C in a 15% H_2/N_2 atmosphere exposed to 15 g m^{-3} benzene for 30 min in humidified steam. Log scale frequencies are presented next to the 0% steam plot.

in polarization resistances, is minimized towards the characteristic initial R_p of the anode. This indicates reduced carbon deposition consistent with the thermodynamic predictions shown in Fig. 2.

3.3. *Effect of steam on anode performance exposed to gasification tar*

In a SOFC, carbon is suppressed by both steam reforming (Eq. (2)) and oxygen ion transport across the zirconia electrolyte (Eq. (1)), which oxidizes carbon formed on the surface of the anode. As discussed earlier, the composition and pretreatment of the anode both play an important role in minimizing the effects of carbon formation on the performance of the fuel cell. Two commercially available fuel cell anodes, Ni/YSZ and Ni/CGO, were studied to compare the effect of steam concentration on the performance and degradation of the anode exposed to 15 g m^{-3} benzene model tar in 15% H_2 for a period of 30 min at OCV.

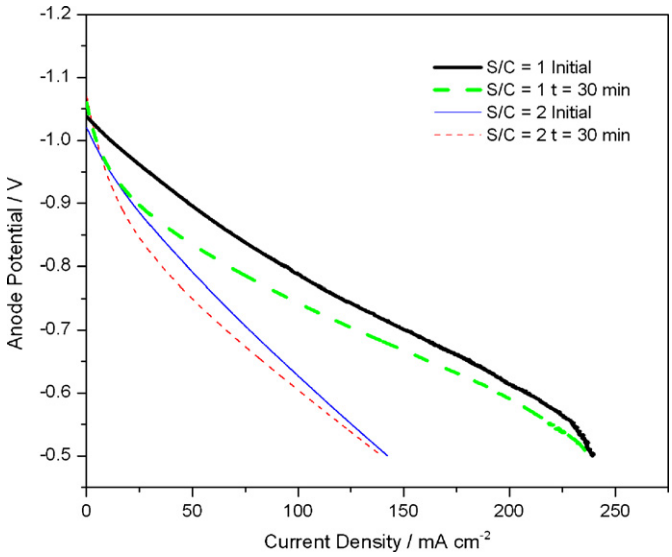

Fig. 6. Initial and final anode polarization curves of SOFCs with Ni–YSZ anodes exposed to 15 g m^{-3} benzene as model tar in a 15% H_2/N_2 atmosphere at 765 °C for 30 min at OCV in humidified steam at two S/C ratios.

3.3.1. Steam reforming of tars over Ni/YSZ anodes

The anode degradation and performance characteristics of separate Ni/YSZ anodes after exposure to 15 g m^{-3} benzene as model tar in 15% H_2 and steam concentrations from 2.5% to 7.5% for 30 min are shown in Figs. 5 and 6. Fig. 5 shows how the addition of humidified steam up to 7.5% (S/C = 3) decreases the polarization resistance of the Ni/YSZ anode after tar exposure, which shows reduced degradation of the cell caused by carbon deposition. These experiments were conducted at OCV, and therefore the predominant mechanism for carbon removal is by steam reforming rather than direct oxidation through oxygen ion transport. The high initial ohmic resistance of the anode may be explained by nickel particle agglomeration following NiO reduction at elevated temperatures, as suggested in Blennow et al. [34].

Comparisons of anode performance are made in Fig. 6 for S/C ratios of 1 and 2. The increase in steam concentration was found to reduce the degree of degradation in anode kinetics associated with the initial response to anode polarization, coinciding with reduced polarization resistances in Fig. 5. However cell degradation from carbon deposits was still severe in high steam concentrations. At higher current densities along the polarization curve, approaching anode potentials of 0.5 V, anode performance approaches that at the initial state prior to tar exposure. Similar effects were observed in dry conditions shown in Fig. 3. This may be the consequence of electrochemical oxidation of deposited carbon at elevated current densities. Visual observations of the cells also showed a decrease in carbon formation with increased steam content, though cell damage due to cermet expansion and anode separation from the electrolyte still occurred at S/C = 3. By comparison with dry operating conditions, it is clear that the addition of steam above a S/C ratio of 1 greatly inhibits the formation of carbon from biomass gasification tars on Ni/YSZ anodes, but does not fully prevent carbon formation as might be expected from the thermodynamic calculations.

3.3.2. Steam reforming of tar over Ni/CGO anodes

As discussed above, steam injection has been shown to be an effective method to reduce carbon formation on Ni/YSZ anodes. However, despite operating the cell well above the thermodynamic threshold for carbon formation at S/C ratios approaching 3 [14], the formation of carbon was still evident, leading to deactivation and degradation of the fuel cell anode.

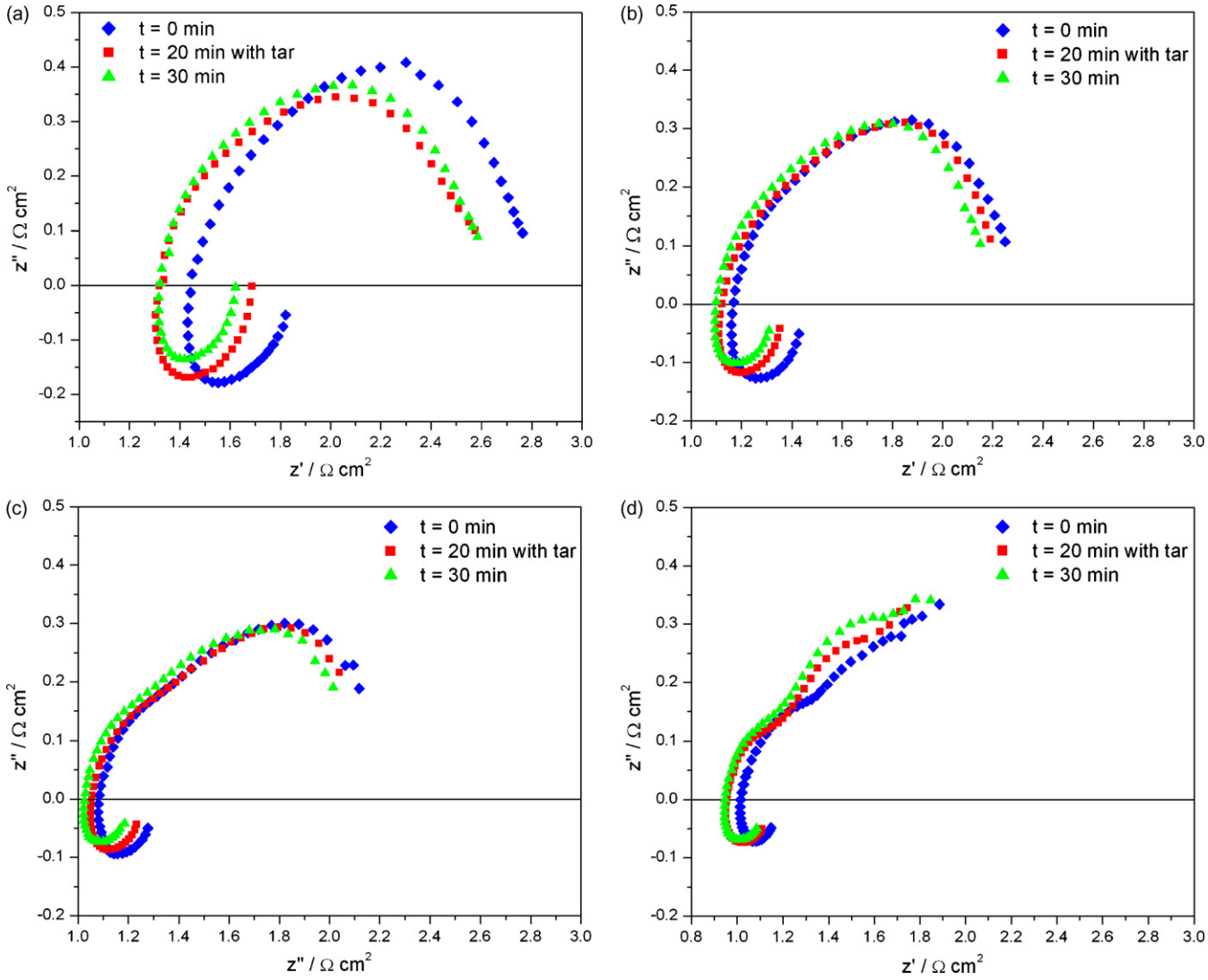

Fig. 7. (a) Impedance spectra of Ni/CGO anodes operating at 765 °C in a 15% H_2/N_2 atmosphere exposed to 15 g m^{-3} benzene for 30 min in 7.5% humidified steam. (b) Impedance spectra of Ni/CGO anodes operating at 765 °C in a 15% H_2/N_2 atmosphere exposed to 15 g m^{-3} benzene for 30 min in 5.0% humidified steam. (c) Impedance spectra of Ni/CGO anodes operating at 765 °C in a 15% H_2/N_2 atmosphere exposed to 15 g m^{-3} benzene for 30 min in 2.5% humidified steam. (d) Impedance spectra of Ni/CGO anodes operating at 765 °C in a 15% H_2/N_2 atmosphere exposed to 15 g m^{-3} benzene for 30 min in 1.0% humidified steam.

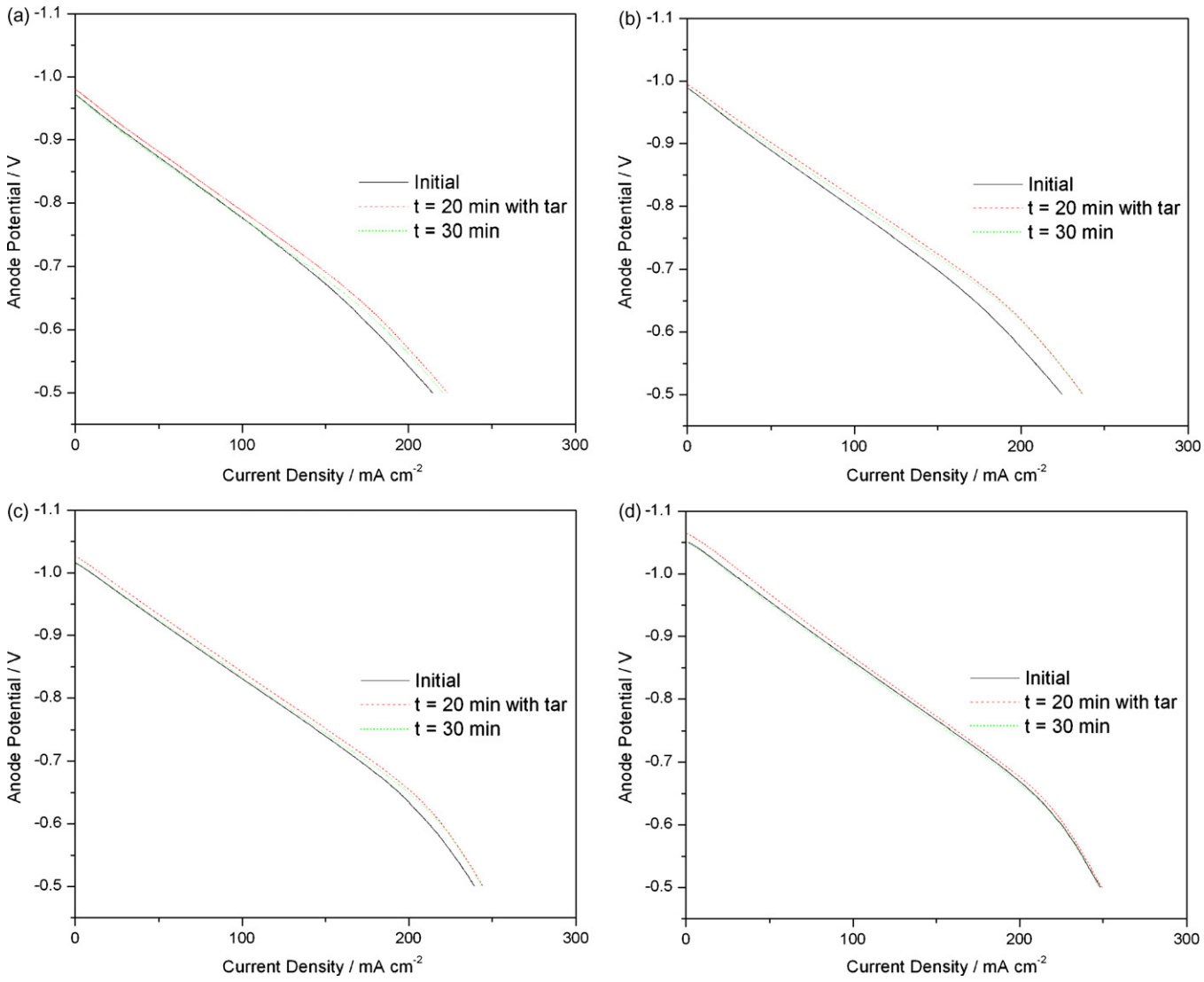

Fig. 8. (a) Polarization curve of Ni/CGO anode operating at 765 °C in a 15% H_2/N_2 atmosphere exposed to 15 g m^{-3} benzene for 30 min in 7.5% humidified steam. (b) Polarization curve of Ni/CGO anode operating at 765 °C in a 15% H_2/N_2 atmosphere exposed to 15 g m^{-3} benzene for 30 min in 5.0% humidified steam. (c) Polarization curve of Ni/CGO anode operating at 765 °C in a 15% H_2/N_2 atmosphere exposed to 15 g m^{-3} benzene for 30 min in 2.5% humidified steam. (d) Polarization curve of Ni/CGO anode operating at 765 °C in a 15% H_2/N_2 atmosphere exposed to 15 g m^{-3} benzene for 30 min in 1.0% humidified steam.

Cerium oxide is a key component in catalysts for reactions involving the oxidation of hydrocarbons because of its high concentration of highly mobile oxygen vacancies that act as a sink for oxygen involved in reactions at the surface of the catalyst. The surface reaction of hydrocarbon species with oxygen in the CGO was found to be the rate controlling step, while oxygen is replenished by a more facile reaction between steam and CGO [35]. It had been expected that the CGO based anode catalyst would show less carbon formation than its YSZ equivalent, as ceria is well known for its ability to resist carbon deposition and to catalyze the oxidation of carbon [35,36]. To test this, a Ni/CGO anode supported on a YSZ electrolyte containing an LSM-20 cathode and reference electrode was used. The effects of anode degradation and performance characteristics of the Ni/CGO anodes after exposure to 15 g m^{-3} benzene model tar for 30 min at 765 °C in 15% H_2 and varying amounts of steam at OCV are shown in Figs. 7 and 8. Fig. 7a–d shows the impedance characteristics of the anode before tar exposure, while operating on tars at t = 20 min, and after 30 min exposure to tar at humidified steam concentrations of 7.5%, 5%, 2.5%, and 1% successively. The cell was initially exposed to tars in 7.5% humidified steam to minimize the effects of carbon formation on using a single cell for consecutive experiments. The initial exposure to tars at this high steam concentration showed a decrease in the series resistance, and a negligible change in the polarization resistance of the anode in comparison with the initial conditions of the cell. This can be attributed to some degree of carbon deposition and/or microstructural changes in the anode leading to increased conductivity. However, if some carbon was formed, it did not affect the electrochemical response seen in the polarization resistance of the anode. Further exposure to tars in humidified steam concentrations down to 2.5% did not show any significant changes in anode polarization resistance after exposure to tars. The R_p of the anode operating in 1% humidified steam is not presented as it could not be accurately determined. It can be seen that the change in series resistance with tar exposure decreases as the steam concentration approaches 2.5% (~S/C = 1). However lowering the steam content below the thermodynamic threshold for carbon formation led to a larger change with a reduction in R_s after exposure to tar, indicating the deposition of carbon on the anode. As a single cell was used for these experiments, the effects of R_s were minimized after consecutive experiments due to the carbon that was initially deposited on first exposure to tars. These results are further tabulated in Table 2.

Table 2
Series and polarization resistance of Ni/CGO anode before, during (t = 20 min), and after operating on 15 g m^{-3} benzene as model tar in 15% H_2 atmosphere in humidified steam for 30 min at OCV.

Humidified steam	Initial	Operating with tar	After tar exposure
Series resistance (Ω cm^2)			
7.5%	1.45	1.31	1.31
5.0%	1.18	1.11	1.1
2.5%	1.08	1.05	1.02
1.0%	1.02	0.879	0.875
Polarization resistance (Ω cm^2)			
7.5%	1.36	1.34	1.34
5.0%	1.12	1.11	1.1
2.5%	1.04	1.05	1
1.0%	–	–	–

Anode potentials for the initial performance of the anode, and following a 30 min exposure to 15 g m^{-3} benzene model tar in humidified steam concentrations from 7.5% to 1%, are shown in Fig. 8a–d, respectively. Degradation rates of the Ni/CGO anodes in the absence of tars were insignificant with rates of 0.0036 and 0.0030 Ω cm^2 h^{-1} for the R_s and R_p, respectively. The effects of steam on anode performance can be seen by comparing the initial conditions at each steam concentration in Fig. 8. Increasing steam concentration leads to increased series resistance and a reduction in OCV, independent of possible carbon that may have formed in low quantities. In separate fuel cell experiments (not shown) under conditions of 15% H_2 and varying steam only, changes in R_p and anode reaction kinetics were found to be negligible. Therefore the decrease in anode performance can be explained by a downward shift in the polarization curve, a result of reduced OCV from the increase in steam concentration.

Comparing Fig. 8a and b, it would have been expected that high humidified steam contents above 7.5% would show the largest improvement in anode performance in comparison to subsequent experiments at lower steam levels, as the fuel cell was operating well above the thermodynamic boundary for carbon formation. However the change in anode potential after tar exposure in 7.5% steam throughout the polarization curve was less than that of the 5% humidified steam experiment. This may be the result of alteration to the anode microstructure due to the initial exposure to and reforming steps of the heavy hydrocarbon fuel. In addition, the dilution of fuel from the high steam content may have affected mass transport within the cell at high current densities along the polarization curve.

Fig. 8a–d also shows that, similar to the impedance data in Fig. 7a–d, the effect of operating the fuel cell with benzene as model tar for 30 min had little effect on the current–potential curve of the anode. It was evident however that the OCV did increase while the anode was exposed to tar, consistent with previous results [5] showing that low concentrations of tar compounds act as a fuel to the fuel cell. Following removal of the tar from the gas stream, the OCV immediately returned back to its initial condition suggesting, along with R_p data from Fig. 7, that the electrochemical response of the cell was not adversely affected. One explanation for the increase in performance after exposure to tars in steam contents >1%, as shown in Fig. 9, is that as suggested by Coll et al., benzene is adsorbed with water onto the surface of the nickel until all carbon atoms are converted to CO or CO_2 [37]. As the impedance spectra and polarization curves were taken immediately after tars were removed from the gas stream, unconverted tar may have still been absorbed on the surface of the anode. The continued reforming of the condensed tar to CO, providing an increase in local fuel concentration, may offer an explanation for the increase in performance.

The change in Ni/CGO anode performance, measured as the change in anode potential between initial conditions and after 30 min exposure to tars, for steam contents from 1% to 5% at current densities along the polarization curve are shown in Fig. 9. Performance changes at 7.5% humidified steam are not shown due to the changes from the initial exposure to tars as discussed above. As shown in Fig. 8, there were insignificant changes from the initial state of the polarization curve at current densities less than 100 mA cm^{-2}. Therefore, Fig. 9 shows the increase in performance as a function of anode potential along the polarization curve from 100 to 200 mA cm^{-2}. Anode potential increased after exposure to 2.5% and 5% humidified steam, however performance began to decrease as steam decreased towards 1%, within the thermodynamically stable region for carbon formation. As suggested by thermodynamic calculations [14], as the steam content falls below a S/C of 1 (~2.5% humidified steam) the deposition of carbon becomes thermodynamically preferred. Small deposits of carbon may increase anode conductivity and performance as discussed herein and in [20,21]. However high quantities of carbon lead to increased anode polarization resistances, reduced mass transport of fuel to the triple phase boundary, and degradation of the cell. As seen here, the low steam content of 1% led to reduced anode performance, most likely from the onset of carbon deposits arising from exposure to tar in a thermodynamically stable region for carbon formation. By contrast, steam levels above the thermodynamic threshold for coke formation show an increase in performance, from the possible reforming of condensed tar.

The fuel cell was removed from the SOFC test apparatus and the anode microstructure was analyzed for carbon deposits and anode degradation using a scanning electron microscope (SEM). In contrast with the Ni/YSZ anode, visual inspection of the cell indicated no significant damage. Some carbon formation was evident at the outer edge of the anode electrolyte surface. The microstructure shown in Fig. 10a does not show any evidence of carbon, this held true for the majority of the surface of the anode. A few areas near the edge of the anode were found to have small patches of carbon deposits as shown in Fig. 10b. This may be the result of internal flow channels within the apparatus, in the contact area between the current collector and the electrode.

It should be noted that after four subsequent exposures of benzene model tar in decreasing steam, the amount of carbon formed on the anode was not sufficient to cause significant performance degradation. The carbon may not have begun to form until the

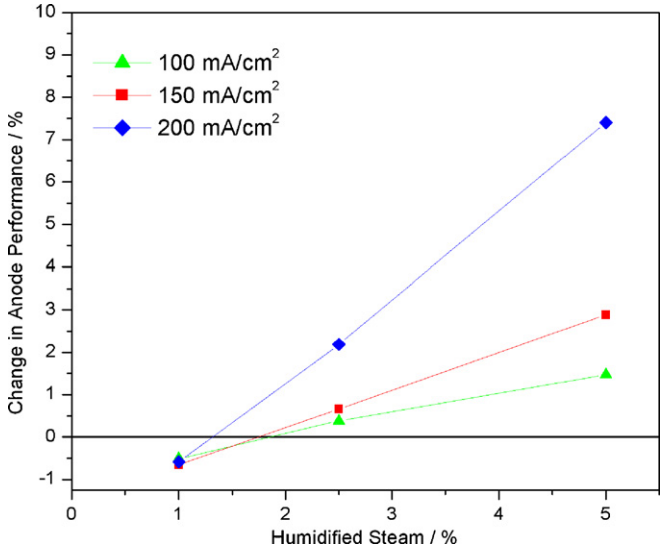

Fig. 9. Change in Ni/CGO anode performance measured at fixed current densities operating in 15% H_2 at 765 °C with varying steam concentrations after 30 min exposure to 15 g m^{-3} benzene as model tar.

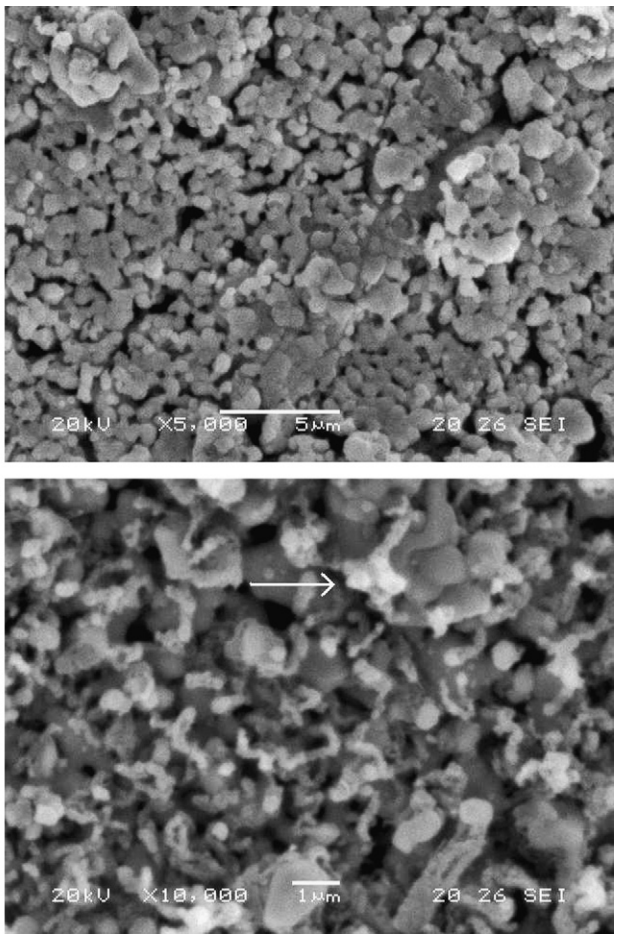

Fig. 10. SEM micrograph of Ni/CGO anode after four 30 min exposures to 15 g m^{-3} tar in humidified steam levels of 7.5–1% in 15% H_2 operating at 765 °C. (a) Area of anode not containing carbon and (b) carbon formed (shown by the arrow) at the edge of the anode electrolyte interface.

steam content dropped below the thermodynamic boundary for carbon formation. This is in sharp contrast to the microstructure of the Ni/YSZ anode after a single 30 min exposure to 5 g m^{-3} benzene model tar in 5% steam and 40% H_2 shown in Fig. 11. Though the H_2 gas composition was higher (as part of a separate study), it does show carbon deposits within the Ni/YSZ cermet structure. As shown in Fig. 5 this led to significantly higher R_p and cell degradation as compared to the Ni/CGO anodes, even though the fuel cell was run well outside the region in which carbon is thermodynamically stable. Previous results in [14] found that Ni/CGO catalyst material (as used in this paper) exhibited slightly more carbon when exposed to benzene in a packed bed than the Ni/YSZ counterpart. This may have been an effect of the surface area and nickel content of the materials used. As a sintered material in a working SOFC anode, results were different, showing that the Ni/YSZ anodes were much more susceptible to carbon deposition. Therefore it may be concluded that the composition and structure of the anode has a significant role in the suppression of carbon formation from such biomass gasification tar compounds.

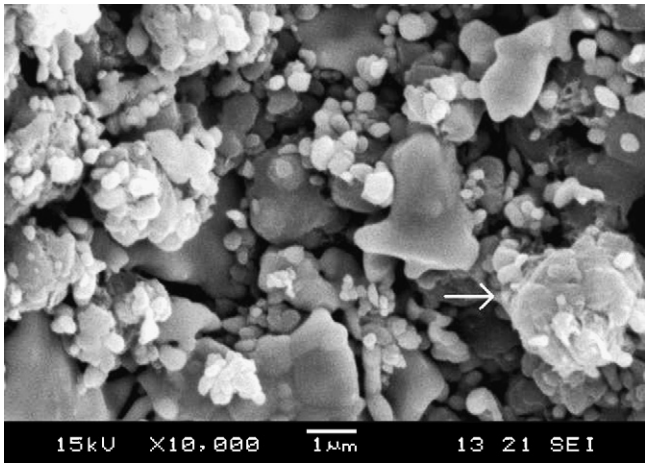

Fig. 11. SEM micrograph of Ni/YSZ anode after a single 30 min exposures to 5 g m^{-3} tar in 5% humidified steam in 40% H_2 operating at 765 °C.

4. Conclusions

An experimental study has been conducted on the mitigation of carbon formation arising from the exposure of Ni/YSZ and Ni/CGO SOFC anodes to biomass gasification tars. Carbon formation and cell degradation were reduced through means of steam reforming and partial oxidation of benzene model tar via the transport of oxygen ions to the anode while operating the fuel cell under closed circuit conditions.

Partial oxidation of the tar can occur by oxygen ions transported from the cathode to the anode under load. The most efficient point for partial oxidation of the carbonaceous species occurs at the threshold current density, at which carbon formation is no longer favored. Thermodynamic models for a SOFC operating in dry conditions exposed to 15 g m^{-3} gasification tar suggest that a current density of >365 mA cm^{-2} is required to suppress the formation of carbon based on the experimental conditions used in this study. Under similar experimental conditions, cell degradation, measured by impedance spectroscopy, was minimized as cell load was increased towards the threshold current density.

The lateral conductivity of the Ni/YSZ anode was found to be quite poor, resulting in high polarization resistances before exposure to tar. However it was shown that R_p decreased after exposure to tar with increased steam content, reducing anode degradation. However, even under high steam contents, carbon formation was still sufficient to cause irreversible damage to the anode.

Conversely, the electrochemical response of the Ni/CGO anode was unaffected by the exposure to benzene as model tar in steam. The R_s of the cell did, however, decrease after each subsequent tar exposure, most prominently after the initial exposure in 7.5% steam. The initial exposure to tars led to possible microstructural changes, or small amounts of carbon deposits. The Ni/CGO anode performance was shown to increase after exposure to tars in steam concentrations greater than the thermodynamic threshold for carbon formation. This may have been a result of continued reforming/oxidation of the condensed tar on the anode while obtaining the impedance and polarization curve.

It may be concluded that the structure and composition of the anode, and the operational characteristics of the SOFC, have a significant role in the suppression of carbon formation from biomass gasification tars, with Ni/CGO anodes being more resilient to carbon formation.

References

[1] L. Fryda, K.D. Panopoulos, E. Kakaras, Energy Conversion and Management 49 (2008) 281–290.
[2] A.O. Omosun, A. Bauen, N.P. Brandon, C.S. Adjiman, D. Hart, Journal of Power Sources 131 (2004) 96–106.
[3] T. Seitarides, C. Athanasiou, A. Zabaniotou, Renewable and Sustainable Energy Reviews 12 (2008) 1251–1276.
[4] S. Vasileiadis, Z. Ziaka-Vasileiadou, Chemical Engineering Science 59 (2004) 4853–4859.

[5] J. Mermelstein, M. Millan, N.P. Brandon, Chemical Engineering Science 64 (2009) 492–500.
[6] M. Ni, D.Y.C. Leung, M.K.H. Leung, K. Sumathy, Fuel Processing Technology 87 (2006) 461–472.
[7] P. McKendry, Bioresource Technology 83 (2002) 55–63.
[8] Y. Cao, Y. Wang, J.T. Riley, W.-P. Pan, Fuel Processing Technology 87 (2006) 343–353.
[9] D. Singh, E. Hernandez-Pacheco, P.N. Hutton, N. Patel, M.D. Mann, Journal of Power Sources 142 (2005) 194–199.
[10] H. He, J.M. Hill, Applied Catalysis A: General 317 (2007) 284–292.
[11] C.M. Finnerty, N.J. Coe, R.H. Cunningham, R.M. Ormerod, Catalysis Today 46 (1998) 137–145.
[12] J. Macek, B. Novosel, M. Marinsek, Journal of the European Ceramic Society 27 (2007) 487–491.
[13] R.J. Gorte, J.M. Vohs, Journal of Catalysis 216 (2003) 477–486.
[14] J. Mermelstein, N.P. Brandon, M. Millan, Energy and Fuels, doi:10.1021ef900426g.
[15] K. Ke, A. Gunji, H. Mori, S. Tsuchida, H. Takahashi, K. Ukai, Y. Mizutani, H. Sumi, M. Yokoyama, K. Waki, Solid State Ionics 177 (2006) 541–547.
[16] H. Sumi, K. Ukai, Y. Mizutani, H. Mori, C.-J. Wen, H. Takahashi, O. Yamamoto, Solid State Ionics 174 (2004) 151–156.
[17] K.M. Walters, A.M. Dean, H. Zhu, R.J. Kee, Journal of Power Sources 123 (2003) 182–189.
[18] Y. Shiratori, T. Oshima, K. Sasaki, International Journal of Hydrogen Energy 33 (2008) 6316–6321.
[19] J. Golbert, C.S. Adjiman, N.P. Brandon, Industrial & Engineering Chemistry Research 47 (2008) 7693–7699.
[20] C. Mallon, K. Kendall, Journal of Power Sources 145 (2005) 154–160.
[21] G.-B. Jung, K.-F. Lo, S.-H. Chan, Journal of Solid State Electrochemistry 11 (2007) 1435–1440.
[22] K.O. Christensen, D. Chen, R. Lødeng, A. Holmen, Applied Catalysis A: General 314 (2006) 9–22.
[23] J. Sehested, J.A.P. Gelten, S. Helveg, Applied Catalysis A: General 309 (2006) 237–246.
[24] M.D. Shroff, D.S. Kalakkad, K.E. Coulter, S.D. Kohler, M.S. Harrington, N.B. Jackson, A.G. Sault, A.K. Datye, Journal of Catalysis 156 (1995) 185–207.
[25] D.L. Giltrap, R. McKibbin, G.R.G. Barnes, Solar Energy 74 (2003) 85–91.
[26] T. Reed, Handbook of Biomass Downdraft Gasifier Engine Systems, The Biomass Energy Foundation Press, Golden, Colorado, 1988, pp. 1–99.
[27] P. Vervaeke, F.M.G. Tack, F. Navez, J. Martin, M.G. Verloo, N. Lust, Biomass and Bioenergy 30 (2006) 58–65.
[28] Z.A. Zainal, A. Rifau, G.A. Quadir, K.N. Seetharamu, Biomass and Bioenergy 23 (2002) 283–289.
[29] S. Baron, N. Brandon, A. Atkinson, B. Steele, R. Rudkin, Journal of Power Sources 126 (2004) 58–66.
[30] G.J. Offer, P. Shearing, J.I. Golbert, D.J.L. Brett, A. Atkinson, N.P. Brandon, Electrochimica Acta (2007), doi:10.1016/j.electacta.2008.04.001.
[31] K. Sasaki, Y. Teraoka, Journal of The Electrochemical Society 150 (2003) A885–A888.
[32] z.B.-S.K. Joon-Ho Koh, H.C. Lim, Y.-S. Yoo, Electrochemical and Solid-State Letters 4 (2) (2001) A12–A15.
[33] J.H. Koh, B.S. Kang, H.C. Lim, Y.-S. Yoo, Electrochemical and Solid-State Letters 4 (2) (2001) A12–A15.
[34] P. Blennow, K.K. Hansen, L.R. Wallenberg, M. Mogensen, ECS Transactions 13 (2008) 181–194.
[35] E. Ramirez-Cabrera, A. Atkinson, D. Chadwick, Applied Catalysis B: Environmental 47 (2004) 127–131.
[36] B.T. Kilbourn, Cerium: A Guide to its Roll in Chemical Technology, Molycorp Inc., White Plains, USA, 1992.
[37] R. Coll, J. Salvado, X. Farriol, D. Montane, Fuel Processing Technology 74 (2001) 19–31.